Acta Crystallographica Section D
Biological Crystallography
ISSN 1399-0047

The crystal structure of human mitochondrial 3-ketoacyl-CoA thiolase (T1): insight into the reaction mechanism of its thiolase and thioesterase activities

Tiila-Riikka Kiema,[a] Rajesh K. Harijan,[a] Malgorzata Strozyk,[b] Toshiyuki Fukao,[c] Stefan E. H. Alexson[b] and Rik K. Wierenga[a]*

[a]Faculty of Biochemistry and Molecular Medicine, Biocenter Oulu, University of Oulu, PO Box 3000, FIN-90014 Oulu, Finland, [b]Karolinska Institutet, Department of Laboratory Medicine, Division of Clinical Chemistry, Karolinska University Hospital, SE-141 86 Stockholm, Sweden, and [c]Department of Pediatrics, Graduate School of Medicine, Gifu University, Yanagido 1-1, Gifu 501-1194, Japan

Correspondence e-mail: rik.wierenga@oulu.fi

Received 12 August 2014
Accepted 28 October 2014

PDB references: human mitochondrial 3-ketoacyl-CoA thiolase, 4c2k; complex with CoA, 4c2j

Crystal structures of human mitochondrial 3-ketoacyl-CoA thiolase (hT1) in the apo form and in complex with CoA have been determined at 2.0 Å resolution. The structures confirm the tetrameric quaternary structure of this degradative thiolase. The active site is surprisingly similar to the active site of the *Zoogloea ramigera* biosynthetic tetrameric thiolase (PDB entries 1dm3 and 1m1o) and different from the active site of the peroxisomal dimeric degradative thiolase (PDB entries 1afw and 2iik). A cavity analysis suggests a mode of binding for the fatty-acyl tail in a tunnel lined by the Nβ2–Nα2 loop of the adjacent subunit and the Lα1 helix of the loop domain. Soaking of the apo hT1 crystals with octanoyl-CoA resulted in a crystal structure in complex with CoA owing to the intrinsic acyl-CoA thioesterase activity of hT1. Solution studies confirm that hT1 has low acyl-CoA thioesterase activity for fatty acyl-CoA substrates. The fastest rate is observed for the hydrolysis of butyryl-CoA. It is also shown that T1 has significant biosynthetic thiolase activity, which is predicted to be of physiological importance.

1. Introduction

Thiolases are enzymes which are involved in lipid metabolism, catalysing the biological Claisen condensation and thiolytic cleavage reactions using a cysteine thiol in the active site. Currently, there are six characterized mammalian thiolases with specific functions in lipid metabolism depending on their substrate specificity, catalytic properties and subcellular localization (Fukao, 2002; Anbazhagan *et al.*, 2014). Cytosolic thiolase (CT) and mitochondrial acetoacetyl-CoA thiolase (T2) are short-chain-specific biosynthetic thiolases. CT catalyses the first reaction of the cholesterol-biosynthesis pathway (Middleton, 1974), whereas T2 is involved in ketone-body metabolism (Staack *et al.*, 1978) and isoleucine catabolism (Middleton & Bartlett, 1983; Haapalainen *et al.*, 2007). 3-Ketoacyl-CoA thiolase (T1; Middleton, 1973) and the thiolase dimer of the trifunctional enzyme (TFE; Uchida *et al.*, 1992) catalyse the last step of the mitochondrial β-oxidation pathway. TFE is membrane-associated and is specific for very long chain fatty acids and 2-methyl branched-chain fatty acids (Mao *et al.*, 1995), whereas soluble T1 is specific for medium-chain to long-chain unbranched fatty acids (Staack *et al.*, 1978; Mao *et al.*, 1995; Miyazawa *et al.*, 1981). Peroxisomal 3-ketoacyl-CoA thiolase (AB-thiolase; Antonenkov *et al.*, 1999; Bout *et al.*, 1991) and SCP2-thiolase (Antonenkov *et al.*, 1997) are involved in the peroxisomal β-oxidation of very long and 2-methyl branched fatty acids, respectively. SCP2-thiolase also has a specific function in the bile acid biosynthesis pathway (Antonenkov *et al.*, 1997).

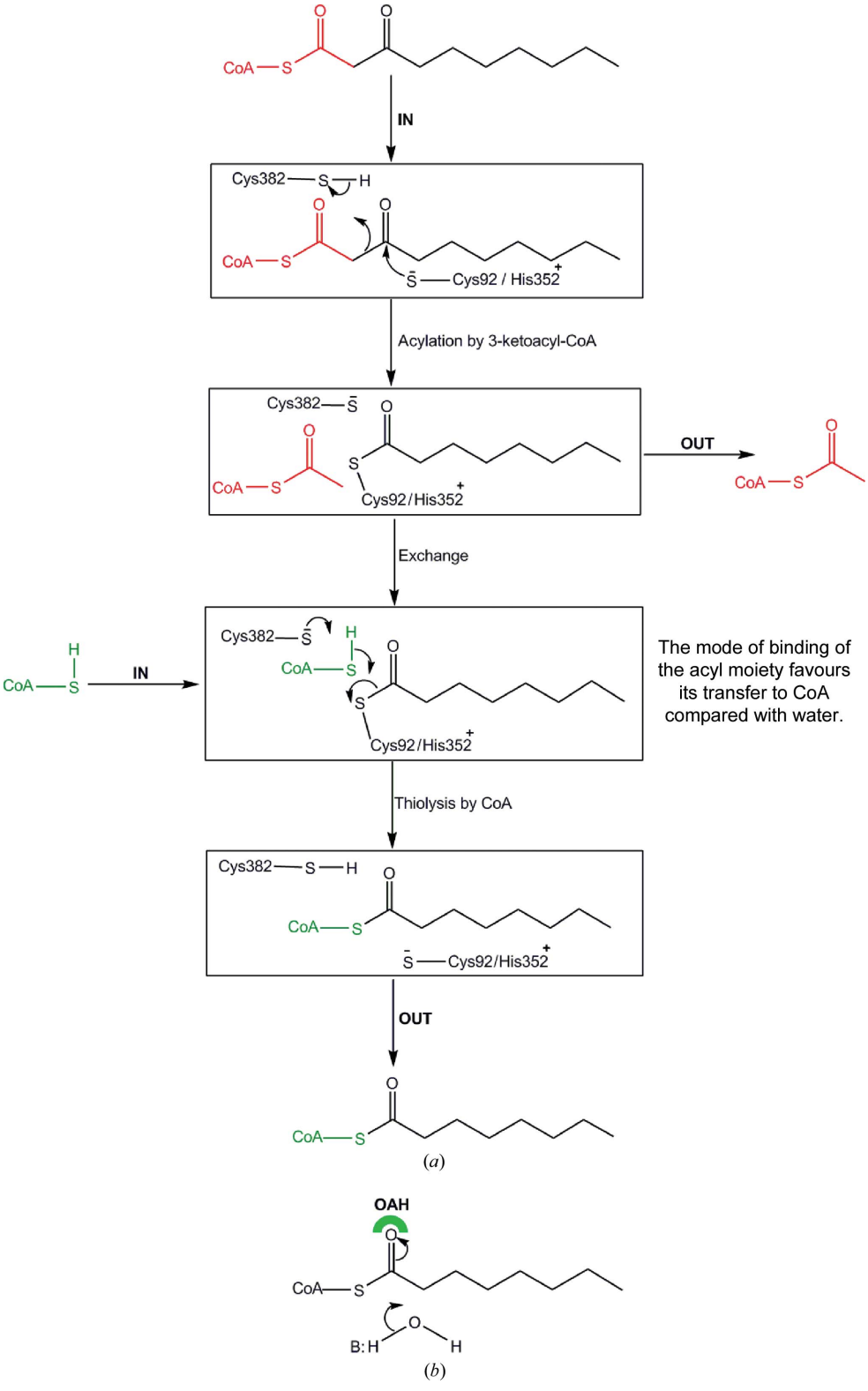

Figure 1
(*a*) Schematic presentation of the degradation of 3-ketodecanoyl-CoA into acetyl-CoA and octanoyl-CoA by human mitochondrial 3-ketoacyl-CoA thiolase. (*b*) Proposed mode of binding of the thioester O atom of the fatty acyl-CoA in OAH1 or OAH2. In this mode of binding a negative charge developing on the thioester O atom is stabilized, thereby facilitating nucleophilic attack by a water molecule on the carbonyl C atom and thus favouring the hydrolysis of the thioester moiety by a water molecule. For an efficient reaction with water it is required that a catalytic base abstracts a proton from this water and donates it to CoA, the leaving group of the thioesterase reaction.

T1 (EC 2.3.1.16) is a tetrameric enzyme of four identical subunits, each of approximately 400 residues (Staack *et al.*, 1978; Uchida *et al.*, 1992; Miyazawa *et al.*, 1981). It catalyses the thiolytic cleavage of medium-chain to long-chain 3-ketoacyl-CoAs to acetyl-CoA and a fatty acyl-CoA shortened by two C atoms. The enzyme-kinetic properties of T1 from bovine liver (Seubert *et al.*, 1968), pig heart (Schulz & Staack, 1981; Gilbert *et al.*, 1981) and rat liver (Uchida *et al.*, 1992; Miyazawa *et al.*, 1981) have been characterized. It has a broad substrate specificity, accepting fatty acyl-CoAs with four to 14 C atoms, with the activity being highest with fatty-acyl chains of six to eight C atoms (Staack *et al.*, 1978; Uchida *et al.*, 1992; Miyazawa *et al.*, 1981). T1 can also catalyse the condensation of two acetyl-CoA molecules into acetoacetyl-CoA (Gilbert *et al.*, 1981). In humans, T1 is particularly abundant in the liver, heart, kidney and adrenal glands (Fukao, 2002).

The thiolase reaction mechanism has been well characterized for the *Zoogloea ramigera* biosynthetic thiolase (Thompson *et al.*, 1989; Williams *et al.*, 1992; Modis & Wierenga, 1999, 2000; Kursula *et al.*, 2002; Meriläinen *et al.*, 2009), which catalyses the condensation of two acetyl-CoA molecules into acetoacetyl-CoA in the poly-3-D-hydroxybutyrate pathway (Masamune *et al.*, 1989). In Fig. 1 the degradative thiolase reaction catalysed by T1 is shown based on the structural and enzymological data of the *Z. ramigera* thiolase. No metal ions or coenzymes are involved in the reaction as a cofactor. Both the thiolytic cleavage and the condensation reaction are catalysed *via* covalent modification of the nucleophilic cysteine (Cys92) and by stabilization of the negatively charged reaction intermediates by oxyanion holes (OAHs; Haapalainen

et al., 2006). The nucleophilic cysteine attacks the β-carbon of the 3-ketoacyl-CoA and becomes covalently modified. Another cysteine, Cys382, acts first as an acid providing a proton for the leaving acetyl-CoA and next as a base abstracting a proton from the incoming CoA. The activated CoA molecule then attacks the carbonyl C atom of the acylated cysteine and the fatty acyl-CoA is released. The cysteine acting as the nucleophile is activated by a conserved histidine residue (His352). This protonated histidine subsequently forms OAH1 together with a water molecule which is hydrogen-bonded to Asn320. The pH optimum of the thiolase reaction is around 8.0 (Schulz & Staack, 1981). The rate-limiting steps are different in the degradative and biosynthetic thiolases (Gilbert *et al.*, 1981; Thompson *et al.*, 1989; Gilbert, 1981; Gehring *et al.*, 1968; Gehring & Lynen, 1972). For T1 the rate-limiting step is the formation of the covalent intermediate both in the degradative and the biosynthetic directions (Gilbert *et al.*, 1981; Gilbert, 1981), whereas for the biosynthetic thiolase the rate-limiting step is the removal of the covalent intermediates (Thompson *et al.*, 1989; Williams *et al.*, 1992) in both directions. Studies of these rate-limiting steps have only been performed with an acetyl group, not for longer fatty-acyl tails.

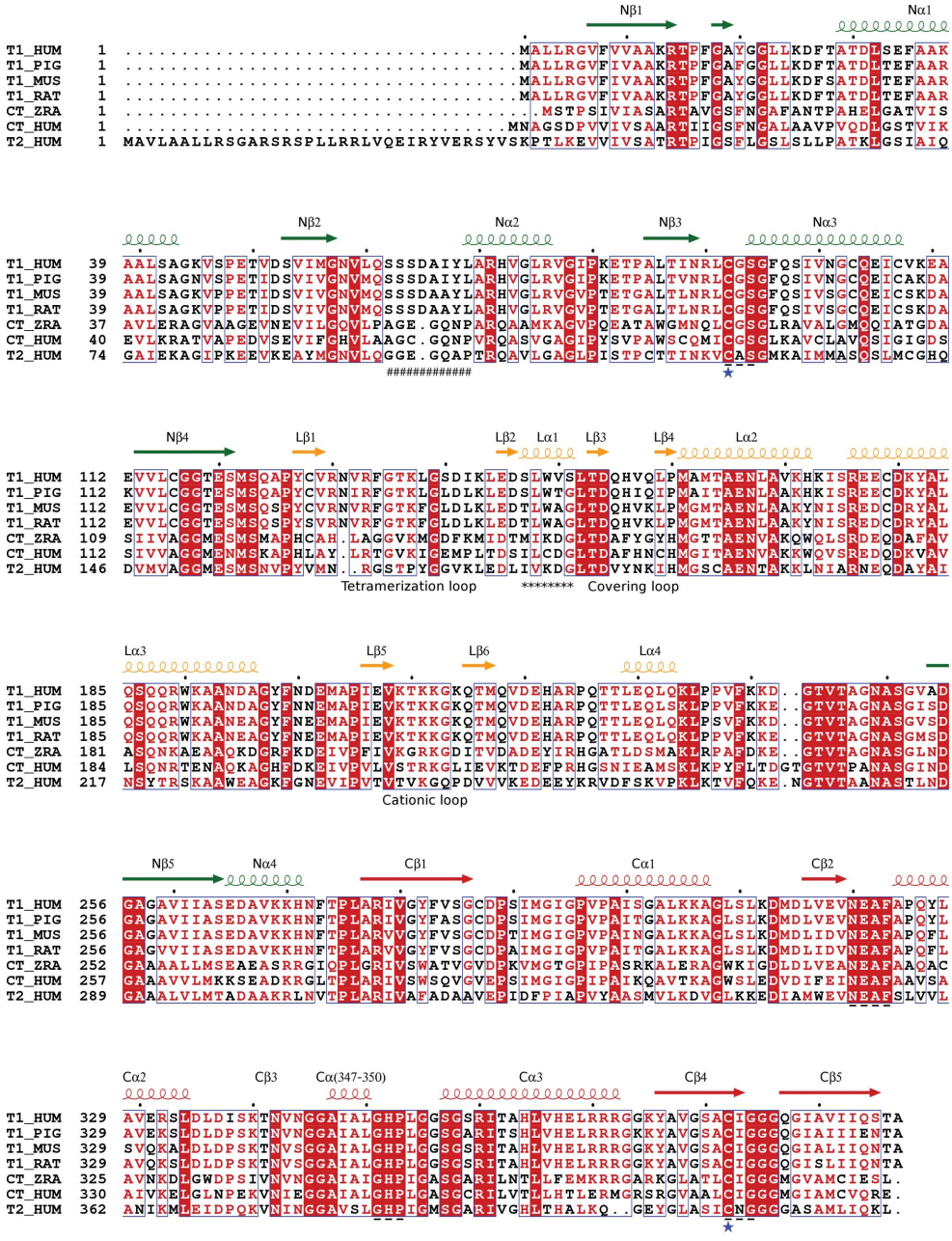

Figure 2
Amino-acid sequence alignment of various tetrameric thiolases. The secondary structure of human mitochondrial 3-ketoacyl-CoA thiolase (hT1) is indicated above the sequence. The N-domain secondary structure is in green, the loop domain (residues Tyr127–Val253) is in yellow and the C-domain is in red. The four catalytic loops are indicated with dashed lines below the sequence and the two active-site cysteines are marked with stars. The two regions in the active site that are different between hT1 and *Z. ramigera* thiolase are highlighted by # (Nβ2–Nα2) and * (Lα1). The amino-acid sequences of T1 (T1_HUM), T2 (T2_HUM) and CT (CT_HUM) from human, T1 from *Sus scrofa* (T1_PIG), *Mus musculus* (T1_MUS) and *Rattus norvegicus* (T1_RAT), and CT from *Z. ramigera* (CT_ZRA) were aligned using *ClustalW* (Larkin *et al.*, 2007) and the figure was prepared with *ESPript* (Gouet *et al.*, 1999).

Currently, the structures of three of the human thiolases have been determined: CT-thiolase (Kursula *et al.*, 2005), T2-thiolase (Haapalainen *et al.*, 2007) and AB-thiolase (PDB entry 2iik; Structural Genomics Consortium, unpublished work). Thiolases share a structurally conserved thiolase core domain composed of topologically similar N-terminal and C-terminal subdomains (each of about 120 residues; Mathieu *et al.*, 1994) and a more variable loop domain (120 residues) with structural features involved in the tetramerization and substrate specificity (Modis & Wierenga, 1999; Mathieu *et al.*, 1994). Thiolases are either dimers or tetramers. Dimerization is mediated *via* the Nβ3 strand of the thiolase core domain, whereas the tetramerization loop at the beginning of the loop domain (Fig. 2) is involved in the dimerization of the two dimers into the typical tetrameric thiolase assembly (Fig. 3). CT-thiolase and T2-thiolase are tetrameric thiolases, whereas AB-thiolase is a dimer.

Here, we report the crystal structure of human T1-thiolase

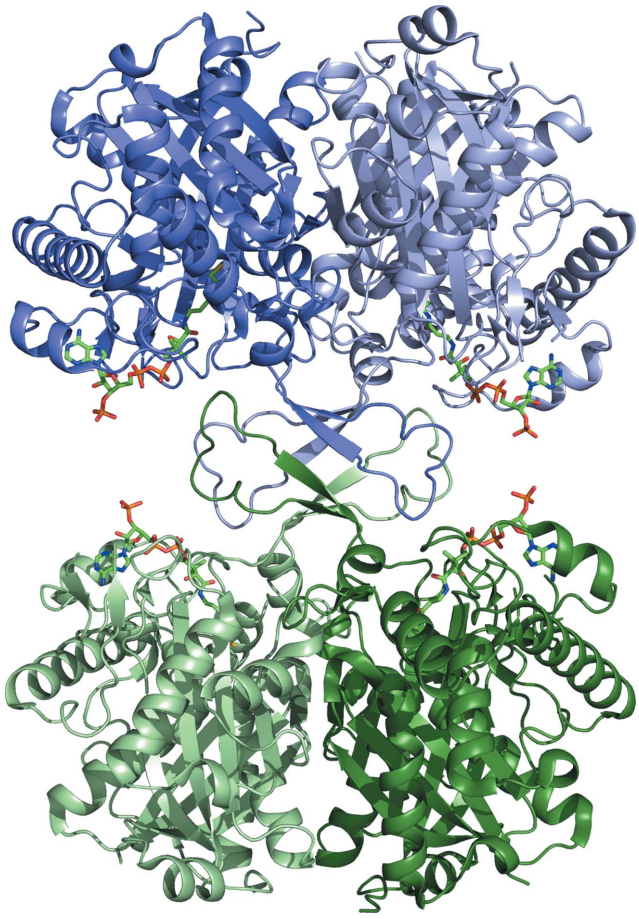

Figure 3
Human mitochondrial 3-ketoacyl-CoA thiolase tetramer in complex with CoA (PDB entry 4c2j). Chains *A*, *B*, *C* and *D* are coloured light green, dark green, dark blue and light blue, respectively.

(hT1) at 2.0 Å resolution. Comparison of the hT1 crystal structure with the biosynthetic short-chain-specific *Z. ramigera* thiolase reveals structural differences in the first α-helix of the loop domain and in the Nβ2–Nα2 loop of the adjacent subunit shaping the putative fatty-acyl tail binding site. Soaking of the apo crystals with octanoyl-CoA resulted in the crystal structure of hT1 in complex with CoA owing to the intrinsic acyl-CoA thioesterase activity of hT1. Characterization of the acyl-CoA thioesterase activity of wild-type hT1 and of the C92A and C92S,C382A variants shows that T1 is able to release free CoA with a slow rate from the fatty acyl-CoAs, with a clear chain-length specificity for medium-chain fatty acyl-CoAs (C4–C10). This acyl-CoA thioesterase activity is dependent on the reduced active-site cysteine, Cys92. The Michaelis–Menten parameters of hT1 in the degradative and biosynthetic directions are also reported using acetoacetyl-CoA and acetyl-CoA as substrates, respectively.

2. Experimental procedures

2.1. Construction of bacterial expression constructs

The human mitochondrial 3-ketoacyl-CoA thiolase cDNA in pGEM vector (Abe *et al.*, 1993) was a kind gift from Dr Ohtake, Japan. The hT1 cDNA was cloned from the pGEM vector using PCR into pETBlue-1 vector (Novagen; pETBlue-1-T1; Sikkilä, 2004). The cDNA was found to contain two sequence conflicts (A169T and A2R), which were mutated to match the mRNA sequence of human T1 (BC001918.1) in the European Nucleotide Archive. The site-directed mutagenesis of the mismatched residues was carried out in two consecutive mutagenesis rounds following the QuikChange mutagenesis protocol (Agilent Technologies Inc.) using *Pfu* DNA polymerase (Stratagene) and 125 ng 5′-GCAGAGAATCTT**GCT**-GTAAAACAC-3′ (mutation site in bold) and its reverse primer (T169A) or 200 ng 5′-GGAGATATACATATG**GCT**C-TGCTCCGAGG-3′ and its reverse primer (R2A) in a final volume of 50 µl. The hT1 cDNA was amplified from the pETBlue-1 vector by PCR in *Pfu* reaction buffer containing 50 ng template DNA, 0.2 m*M* dNTPs, 1 µ*M* 5′-primer (5′-TTAATTCATATGGCTCTGCTCCGAGG-3′) with an *Nde*I restriction site, 1 µ*M* 3′-primer (5′-TTAATTGGATCCTCA-GGCTGTGCTCTG-3′) with a *Bam*HI restriction site and 1.25 U *Pfu* DNA polymerase (Stratagene) in a final volume of 50 µl. Amplified DNA was digested with *Nde*I and *Bam*HI restriction enzymes, ligated into similarly digested pET-15b vector (Novagen) and transformed into DH5α competent cells.

The site-directed mutageneses of the active-site residues were carried out following the QuikChange mutagenesis protocol using Phusion DNA polymerase (Finnzymes) according to the manufacturer's instructions. pET15bT1 served as a template for the generation of the C92A and C382A mutants and pET15bT1C382A served as a template for the C92S,C382A double mutant. The following mutagenesis primers and their reverse primers were used: 5′-GAT-TAATAGGCTC**GCT**GGTTCTGGTTTTC-3′ (C92A), 5′-G-TTGGATCAGCT**GCA**ATTGGAGGTGG-3′ (C382A) and 5′-GATTAATAGGCTC**TCT**GGTTCTGGTTTTC-3′ (C92S). *Dpn*I-digested PCR products were transformed into DH5α or TURBO (Stratagene) competent cells.

DNA sequences were confirmed by DNA sequencing with the DYEnamic ET terminator cycle sequencing kit (GE Healthcare) or with full service sequencing at the Biocenter Oulu DNA-sequencing core facility.

2.2. Bacterial expression and protein purification

For bacterial expression, the pET15bT1, pET15bT1C92A and pET15bT1C92SC382A plasmids were transformed into *Escherichia coli* BL21(DE3) cells (Novagen) with pGro7 plasmid (Takara Inc., Japan) encoding the GroEL and GroES complex. For pre-culture, one colony was transferred into LB medium supplemented with 34 µg ml^{-1} chloramphenicol and 50 µg ml^{-1} carbenicillin and the cells were grown either for 7 h or overnight at 37°C. The overnight-grown pre-culture was diluted 1:100 and the 7 h pre-culture was diluted to an OD_{600} of 0.02 in 1 l M9ZB (1% N-Z-Case Plus, 0.5% NaCl, 0.1% NH_4Cl, 22 m*M* KH_2PO_4, 22 m*M* Na_2HPO_4, 1 m*M* $MgSO_4$, 0.4% glucose) culture medium supplemented with 0.3 mg ml^{-1} arabinose, 34 µg ml^{-1} chloramphenicol and

50 µg ml^{-1} carbenicillin. The cells were grown at 37°C with shaking until the OD_{600} reached 0.6–0.8. Expression of the proteins was induced by adding IPTG to a final concentration of 0.1 m*M* and growth was continued at 20°C overnight. The cells were harvested by centrifugation at 5020*g* for 1 h at 4°C. The bacterial cells were suspended in Ni–NTA lysis buffer (50 m*M* NaH_2PO_4, 0.3 *M* NaCl, 10 m*M* imidazole pH 8.0) and stored at −70°C. Frozen cell suspensions were thawed and diluted to approximately 0.5–1 g of cells in 10 ml buffer supplemented with 1 m*M* DTT. Cells were disrupted by sonication, keeping the sample on ice at all times. The homogenate was cleared by centrifugation at 30 000*g* at 4°C for 45 min. hT1 was purified using Ni–NTA matrix (Qiagen) according to the manufacturer's instructions, with all of the buffers supplemented with 1 m*M* DTT. Fractions containing the hT1 protein were pooled and dialysed against 2 l 20 m*M* sodium phosphate pH 6.8, 1 m*M* EDTA, 1 m*M* DTT overnight at 4°C. The dialysed sample was applied onto Poros 20 SP cation exchanger (Applied Biosystems) equilibrated with 20 m*M* sodium phosphate, 1 m*M* EDTA, 1 m*M* DTT pH 6.8 buffer. The hT1 protein was eluted with a linear NaCl gradient from 0 to 500 m*M* in 14 column volumes, concentrated using an Amicon centrifugal filter (Millipore) at 4°C and applied onto a HiLoad 16/60 Superdex 200 gel-filtration column (GE Healthcare) equilibrated with 25 m*M* Tris–HCl, 50 m*M* KCl, 1 m*M* EDTA, 1 m*M* DTT pH 8.0 buffer. The concentrated purified protein was flash-frozen in small aliquots in liquid nitrogen and stored at −70°C. The protein concentrations were determined by absorption measurements at 280 nm using a NanoDrop (Thermo Scientific) spectrophotometer with the molar extinction coefficient obtained using *ProtParam* (Gasteiger *et al.*, 2005) from the SIB Expasy bioinformatics resources portal (Artimo *et al.*, 2012). In addition to the 397 amino-acid residues (UniProt P42765) of hT1, the expressed hT1 protein had 20 amino-acid residues at the N-terminus containing the His tag and a thrombin cleavage site encoded by the vector (MGSSHHHHH-HSSGLVPRGSH).

Table 1
Data-collection, data-processing and refinement statistics.

Values in parentheses are for the highest resolution shell.

Data set	t1_1	t1_01	t1_07
Crystallization			
Crystallization conditions	100 m*M* MOPS pH 7.2, 15% PEG MME 5000	100 m*M* MES pH 6.6, 14% PEG MME 5000	100 m*M* MES pH 6.6, 15% PEG MME 5000
Soaking	Apo	1 m*M* octanoyl-CoA	Apo
Ligand	—	CoA	—
Data collection			
Beamline	Home source	ID14-4, ESRF	ID14-4, ESRF
Wavelength	1.5418	0.9393	0.9393
Space group	$P2_1$	$P2_1$	$P2_1$
Data processing			
a, *b*, *c* (Å)	55.0, 197.8, 80.3	54.7, 197.2, 80.0	54.7, 196.8, 79.7
α, β, γ (°)	90.0, 104.4, 90.0	90.0, 103.7, 90.0	90.0, 103.8, 90.0
Resolution (Å)	19.84–3.30 (3.35–3.30)	46.74–2.00 (2.10–2.00)	48.17–2.00 (2.10–2.00)
R_{merge}† (%)	10.7 (32.8)	8.5 (39.6)	6.8 (40.7)
$\langle I/\sigma(I)\rangle$‡	19.8 (6.6)	13.7 (3.7)	15.1 (3.1)
Completeness (%)	99.0 (99.5)	99.8 (99.9)	99.6 (99.8)
Multiplicity	5.8 (5.8)	3.8 (3.8)	3.7 (3.7)
Observed reflections	142530 (6318)	413543 (56400)	405314 (55687)
Unique reflections	24753 (1088)	110210 (15019)	109515 (14949)
Wilson *B* factor (Å^2)	28.2	24.8	29.9
Refinement			
R_{work}§/R_{free}¶ (%)		17.23/20.25	19.53/22.89
No. of atoms			
Protein		11655	11712
Ligand		284	140
Waters		807	488
Average *B* factor (Å^2)			
Protein atoms, chain *A*/*B*/*C*/*D*		15.8/17.4/18.3/21.6	22.7/24.4/22.6/25.4
CoA, chain *A*/*B*/*C*/*D*		41.3/41.9/38.8/54.2	
Waters		24.4	27.7
R.m.s. deviations			
Bond lengths (Å)		0.014	0.015
Bond angles (°)		1.5	1.5
Ramachandran plot††, residues in (%)			
Favoured region		99.0	98.6
Allowed region		1.0	1.4
Outlier region		0.0	0.0
PDB code		4c2j	4c2k

† $R_{merge} = \sum_{hkl}\sum_i |I_i(hkl) - \langle I(hkl)\rangle| / \sum_{hkl}\sum_i I_i(hkl)$, where $I_i(hkl)$ is the intensity of the *i*th measurement of reflection *hkl* and $\langle I(hkl)\rangle$ is its mean intensity. ‡ *I* is the integrated intensity and $\sigma(I)$ is its estimated standard deviation. § $R_{work} = \sum_{hkl} ||F_{obs}| - |F_{calc}|| / \sum_{hkl} |F_{obs}|$, where F_{obs} and F_{calc} are the observed and calculated structure factors, respectively. ¶ R_{free} is calculated as for R_{work} but from a randomly selected subset of the data (5%) which were excluded from the refinement calculations. †† Calculated by *PROCHECK*.

2.3. Crystallization and data collection

Initial crystallization conditions were screened with a modified factorial screen (Zeelen *et al.*, 1994) using the sitting-drop vapour-diffusion method in a 96-well plate (Corning) by mixing 1 µl 1.3 mg ml^{-1} hT1 protein in gel-filtration buffer with 1 µl well solution. After optimization of the initial crystallization conditions, crystals were grown in 24-well plates in 100 m*M* MES pH 6.6 or MOPS pH 7.2 and 14–15% monomethyl ether polyethylene glycol (PEG MME 5000) using hanging drops. A 2 µl drop of hT1 protein solution and well solution in a 1:1 ratio was placed above 1 ml well solution. Prior to crystallization, the concentrated protein solution was diluted to 4.4 mg ml^{-1} with 25 m*M* Tris–HCl pH 8.0, 1 m*M* DTT. Crystallization experiments were carried out at 22°C. The crystallization conditions are summarized in Table 1.

The initial hT1 data set (t1_1) was collected using the home-source FR591 rotating-anode X-ray generator (Bruker Nonius) and a MAR345 image-plate detector (MAR Research

GmbH) at 100 K. Before exposure to X-rays the hT1 crystal was quickly treated with vacuum-dried paraffin oil. After initial exposures, the crystal was transferred into a small drop of well solution (100 m*M* MOPS pH 7.2 15% PEG MME 5000) mixed with glycerol in a 1:2.3 ratio and, after a short soak, diffraction data were collected to 3.3 Å resolution at 100 K. The high-resolution apo hT1 data set (t1_07) was collected on beamline ID14-4 at the European Synchrotron Radiation Facility (ESRF), Grenoble, France with a Q315r CCD detector (Area Detector Systems Corporation). The apo hT1 crystals were briefly soaked in a cryosolution consisting of 100 m*M* MES pH 6.6, 15.5% PEG MME 5000, 25% ethylene glycol. In order to obtain the structure of the hT1 complex with a medium-chain fatty acyl-CoA, the hT1 crystals were soaked for 20 min in a soaking solution consisting of 1 m*M* octanoyl-CoA, 14.5% PEG MME 5000, 0.1 *M* MES pH 6.6. Prior to cryocooling in liquid nitrogen, the crystal was incubated for 1 min in a soaking solution additionally containing 25% ethylene glycol. Diffraction data (t1_01) were collected on beamline ID14-4 at the ESRF with a Q315r CCD detector at 100 K.

2.4. Structure determination, model building and refinement

The intensity data of all three data sets were processed using *XDS* (Kabsch, 2010) and converted into an mtz file using *XDSCONV* with a script to run *F2MTZ*. The space group was $P2_1$ and the unit-cell parameters were a = 55.0, b = 197.8, c = 80.3 Å, α = 90.0, β = 104.4, γ = 90.0°. The Matthews coefficient was 2.4 Å^3 Da^{-1} for four subunits per asymmetric unit, with 49% solvent content. The structure was solved by molecular replacement with *Phaser* (McCoy *et al.*, 2007) using the data collected at the home source. The polyalanine model of PDB entry 1dm3 chain *B* (Modis & Wierenga, 2000) was used as a search model. The initial model of the hT1 structure was built manually with *Coot* (Emsley & Cowtan, 2004) and refined using *REFMAC*5 (Murshudov *et al.*, 2011) restrained refinement applying NCS. The free-*R* test set from the home source data was imported into the other data sets collected at the synchrotron. The partially built hT1 model was refined against the data collected from the octanoyl-CoA-soaked crystal (t1_01). The building of the liganded hT1 model consisted of several rounds of manual model building in *Coot*, restrained refinement with *REFMAC*5 applying local autoNCS and validation by *MolProbity* (Chen *et al.*, 2010) and *PROCHECK* (Laskowski *et al.*, 1993). The resulting final hT1 model without the ligand or waters was used as a search model in *Phaser* with the higher resolution apo hT1 data set (t1_07). The apo hT1 model was built, refined and validated using the same protocol as for the liganded hT1 model. The final crystallographic statistics are listed in Table 1. The structural alignments of the hT1, *Z. ramigera* (PDB entries 1dm3 and 1m1o) and yeast peroxisomal (PDB entry 1afw) thiolase structures were made in *Coot* (Emsley & Cowtan, 2004) using the secondary-structure matching (*SSM*) protocol (Krissinel & Henrick, 2004). The structure figures were produced using the *PyMOL* molecular-graphics software (v.1.4.1; Schrödinger).

2.5. Enzyme kinetics of hT1

Enzyme kinetics of hT1 was performed in the degradative and synthetic directions using a Jasco V-660 spectrophotometer (Jasco Inc.) at 25°C. The enzymatic reaction was initiated by adding hT1 after a stable baseline was obtained after 3–5 min. The rate of change in absorbance per minute was calculated using *Spectra Manager* (Jasco Inc.). Measurement of the absorption change in the absence of enzyme was carried out as a control. The total volume of the reaction mixture was 0.5 ml and each activity was measured three times using purified hT1. The concentration of total CoA in the respective substrate solutions was determined by Ellman's test (Riddles *et al.*, 1983) after hydrolysis with 2 *M* hydroxylamine pH 7.0.

In the thiolytic direction, the assay was performed as described previously using the Mg^{2+} method (Haapalainen *et al.*, 2007). The reaction mixture consisted of 50 m*M* Tris–HCl pH 7.8, 25 m*M* $MgCl_2$, 60 µ*M* CoA and a variable concentration of acetoacetyl-CoA from 2 to 60 µ*M* to calculate the K_m and V_{max} of acetoacetyl-CoA degradation. The change in the absorbance was recorded at 303 nm after the addition of 25 ng hT1 to the assay mixture. A molar extinction coefficient of 21 400 M^{-1} cm^{-1} was used for the Mg^{2+}–acetoacetyl-CoA complex (Staack *et al.*, 1978).

In the synthetic direction, the formation of acetoacetyl-CoA was monitored by following the oxidation of NADH in the subsequent reduction reaction of acetoacetyl-CoA to 3-hydroxybutyryl-CoA catalysed by 3-hydroxyacyl-CoA dehydrogenase (HAD; Barycki *et al.*, 1999). The reaction was initiated by adding 200 ng hT1 to a reaction mixture consisting of 50 m*M* Tris–HCl pH 7.8, 40 m*M* KCl, 0.2 m*M* NADH, one unit of HAD (where one unit is the amount of enzyme that converts 1 µmol of substrate per minute), 0.5 m*M* DTT and variable concentrations of acetyl-CoA from 0.1 to 2.5 m*M* to calculate the K_m and V_{max} of the synthetic reaction. The rate of NADH oxidation was measured at 340 nm and the extinction coefficient used for NADH was 6220 M^{-1} cm^{-1} (Horecker & Kornberg, 1948).

2.6. Acyl-CoA thioesterase activity of hT1 and active-site mutants

The thioesterase activity was measured in 200 m*M* KCl, 10 m*M* HEPES pH 8.0 in the presence of 1 m*M* dithiothreitol (DTT) unless otherwise stated in a total volume of 100 µl. To determine the acyl-chain length specificity of the thioesterase activity of hT1, the wild type and the C92A variant of recombinant hT1 were incubated for 15 min with 100 µ*M* acetyl-CoA, propionyl-CoA, butyryl-CoA, hexanoyl-CoA, octanoyl-CoA, decanoyl-CoA, dodecanoyl-CoA or tetradecanoyl-CoA. The effect of DTT on the thioesterase activity of hT1 was determined by incubating the wild type and the C92A and C92S,C382A variants for 30 min with 100 µ*M* octanoyl-CoA in the presence or absence of 1 m*M* DTT. The Michaelis–Menten curve was determined by incubating wild-type hT1 with 10, 20, 40, 80, 100, 150 and 200 µ*M* octanoyl-CoA for 30 min. 20 µl of the incubation mixture was injected onto an HPLC system using a reversed-phase C18 column

(Ultrasphere 10 mm × 25 cm) pre-equilibrated with 100% buffer *A* (100 m*M* ammonium phosphate pH 4). CoA esters and CoA were eluted using a linear gradient of 100% buffer *A* to 100% buffer *B* (50:50 buffer *A*:acetonitrile) for 21 min followed by an isocratic flow with 100% buffer *B* for 15 min. The peak fractions were detected by a UV detector at 260 nm and were analyzed using the *Chromelion* software (Dionex, Thermo Fisher Scientific). The remaining substrates and the formed products were quantitated by peak-area integration using standard curves for CoA.

3. Results and discussions

3.1. Enzyme activity and kinetics

hT1 was overexpressed in a soluble and active form in *E. coli* when coexpressed with the GroEL–GroES complex and was purified to apparent homogeneity. The enzyme-kinetic properties of hT1 were determined in the degradative and biosynthetic directions (Table 2). The K_m and k_{cat} values for the degradation of acetoaceyl-CoA were 9.2 μ*M* and 14.8 ± 0.5 s^{-1}, respectively, and those for the formation of acetoacetyl-CoA were 250 ± 60 μ*M* and 1.4 ± 0.1 s^{-1}, respectively. The observed enzyme-kinetic values for hT1 are consistent with the previously reported activity for pig (Staack *et al.*, 1978; Gilbert *et al.*, 1981) and rat T1 (Miyazawa *et al.*, 1981). hT1 is also a competent biosynthetic thiolase, having very similar K_m and k_{cat} values to those for T2 (K_m = 508 ± 127 μ*M* and k_{cat} = 3.5 ± 0.1 s^{-1}; Haapalainen *et al.*, 2007), which is thought to be responsible for the formation of ketone bodies in the liver as well as for their utilization in the extrahepatic tissues (Middleton & Bartlett, 1983; Fukao *et al.*, 1997).

3.2. Crystallization, structure determination and model quality

The high-resolution structures of apo and CoA-complexed hT1 were determined using crystals grown at pH 6.6 using 15% PEG MME 5000, as described in Table 1. Both structures were solved and refined at 2.0 Å resolution (Table 1). Soaking of the apo hT1 crystals with 1 m*M* octanoyl-CoA resulted in the crystal structure of hT1 in complex with CoA owing to the intrinsic thioesterase activity of hT1. The structure was solved using a *Z. ramigera* biosynthetic thiolase monomer as a search model in molecular-replacement calculations, resulting in four monomers (*A*–*D*) in the asymmetric unit forming a biological tetramer. Chain *A* and chain *B* form a tight dimer, as do chain *C* and chain *D*. The *AB* dimer interacts with the *CD* dimer and this interaction is mediated by the tetramerization loops of each subunit (Modis & Wierenga, 1999). Nearly complete models of hT1 were built with good geometry and no outliers in the Ramachandran plots (Table 1). The apo hT1 model chain *A* contains residues 2–396. The density for the first 20 amino acids containing the His tag and the thrombin cleavage site is not visible in any of the chains except for three residues in chain *D*, which contains residues −2–397. In chains *B* and *C* there is a break in the main chain. Lys211 and Lys212 at the tip of the protruding cationic hairpin loop are missing (Fig. 2; Haapalainen *et al.*, 2007; Kursula *et al.*, 2005). In the CoA-bound structure all of the polypeptide chains have a break in the main chain in the cationic hairpin loop. Chains *A* and *C* contain residues 0–209 and 214–396, whereas chain *B* contains residues −1–208 and 214–397 and chain *D* contains residues −2–209 and 214–396. Apart from the cationic loop, it can be noted that the tetramerization loop also has high *B* factors. Four residues have ψ and φ angles outside the preferred region but within the allowed regions. These residues fit well into the density. These residues are Val59 ($\psi \simeq -60^\circ$, $\varphi \simeq -95^\circ$), Leu91 ($\psi \simeq -130^\circ$, $\varphi \simeq 44^\circ$), Asp141 ($\psi \simeq 76^\circ$, $\varphi \simeq -106^\circ$) and Gln218 ($\psi \simeq 19^\circ$, $\varphi \simeq -146^\circ$). Val59 in the N$\beta$2–N$\alpha$2 loop is buried at the dimer interface. Leu91 is just before the catalytic Cys92 and its side chain is buried at the dimer interface. Asp141 is in the tetramerization loop. Gln218 is at the end of the cationic hairpin loop and interacts with Pro205, which is at the beginning of this loop.

Table 2
Enzyme-kinetic data for hT1 in the degradative and synthetic directions using acetoacetyl-CoA and acetyl-CoA as substrates, respectively.

Substrate	K_m (μ*M*)	k_{cat} (s^{-1})
Acetoacetyl-CoA	9.2 ± 0.9	14.8 ± 0.5
Acetyl-CoA	250 ± 60	1.4 ± 0.1

3.3. Comparison of chains in the models

The four subunits in the apo and the CoA-bound models are very similar. The r.m.s.d. values between the C^α atoms of different subunits vary from 0.1 to 0.3 Å in the apo structure and from 0.1 to 0.2 Å in the CoA-bound structure. The lowest r.m.s.d. values are between chain *A* and chain *D* and the highest are between chain *A* and chain *B*.

The binding of the ligand does not cause any major changes in the hT1 structure. The apo and the CoA-bound structures are very similar; the r.m.s.d. value for the whole tetramer is only 0.3 Å. The r.m.s.d. value between the apo structure (PDB entry 4c2k) chain *A* and the CoA-bound structure (PDB entry 4c2j) chain *C* is 0.2 Å. In the CoA-bound structure the active-site nucleophilic cysteine Cys92 is oxidized to hydroxycysteine, whereas in the apo structure it is unmodified. The nucleophilic cysteine is apparently more sensitive to oxidation in the presence of CoA, which has also been observed in structural studies of other thiolases. The cationic hairpin loop has high *B* factors and is only visible in the apo structure in chains *A* and *D*.

3.4. Description of the structure

The overall fold of the hT1 monomer and the packing of the tetramer (Fig. 3) are the same as in the *Z. ramigera* biosynthetic thiolase and other tetrameric biosynthetic thiolases (CT and T2). The N-terminal part of the hT1 core domain has the '$\beta\alpha\beta\alpha\beta\alpha\beta\beta$' topology in which the β-strands fold into a five-stranded mixed β-sheet sandwiched between α-helices. The Nβ3 strand mediates the dimerization of the thiolase monomers, forming an antiparallel pair of strands across the

dimer twofold axis. The C-terminal part of the hT1 core domain has a four-stranded mixed β-sheet lacking β-strand 3. The residues Thr331-Asn332-Val333 correspond to the Cβ3 region of the *Z. ramigera* thiolase. The loop domain (Tyr127–Val253) extending out from the N-terminal β-sheet and inserting between Nβ4 and Nβ5 is mainly α-helical and folds on top of the thiolase core domain. The loop domain is important for the thiolase function. It is involved in CoA binding and contains structural features that determine the substrate specificity (Mathieu *et al.*, 1997). In hT1, as in the other tetrameric thiolases, the loop domain also contains the tetramerization loop (Tyr127–Asp146). It protrudes out of the bulk of the thiolase fold and mediates tetramer formation by forming a cage-like structure between the opposing thiolase dimers (Modis & Wierenga, 1999), giving it the typical shape of the thiolase tetramer (Fig. 3). The tetramerization loops of the opposing subunits of hT1 cross over to the other dimer pair in such a way that Leu138 at the tip of the tetramerization loop in chain *A* points into the substrate-binding site of chain *D* and so on (Leu138 in subunit *A* is placed between Trp149 and Tyr20 of subunit *D* at a van der Waals distance of 3.6–3.9 Å).

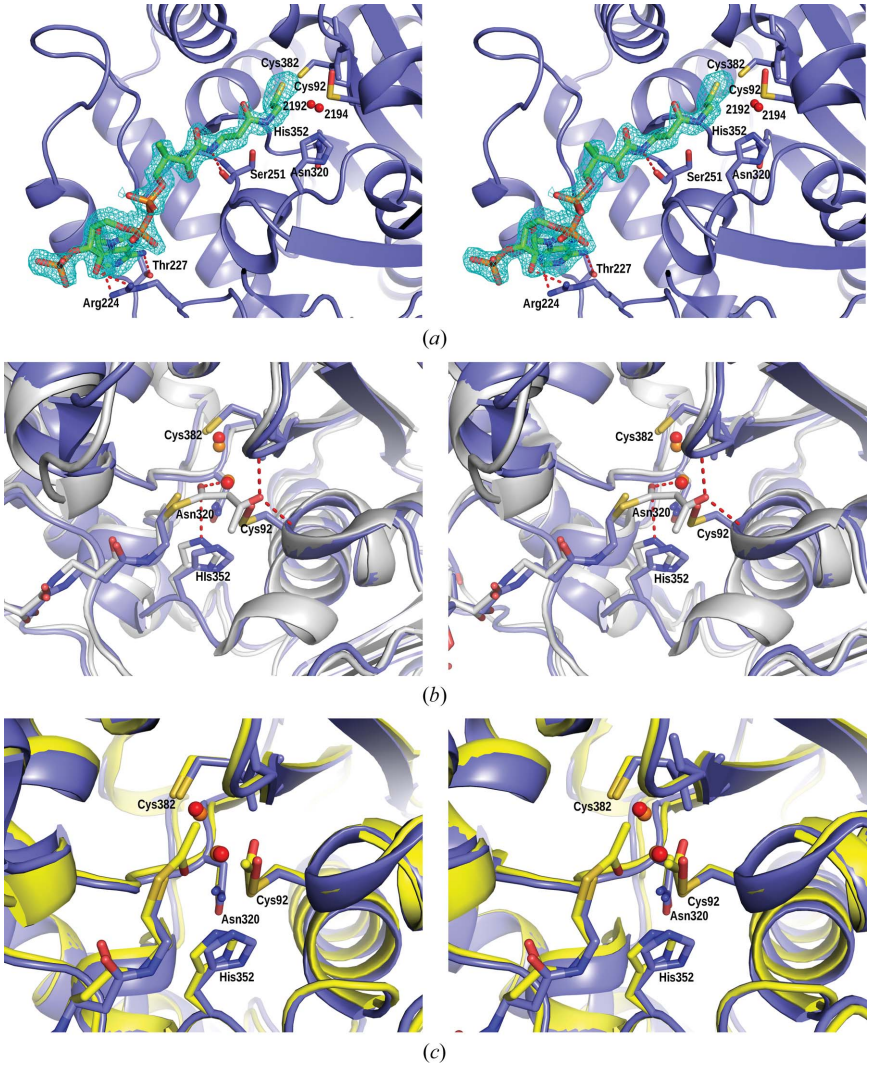

Figure 4
(*a*) Stereo figure of the interactions of human mitochondrial 3-ketoacyl-CoA thiolase chain *C* and the CoA molecule together with the $2F_o - F_c$ map constructed at 1σ. Arg224 interacts with the adenine moiety of the CoA molecule and Thr227 is hydrogen-bonded to the N6A atom of CoA. The carbonyl O atom of Ser251 is hydrogen-bonded to the N8P atom of the pantetheine part of the CoA molecule. The two conserved active-site water molecules and the four active-site residues Cys92, Asn320, His352 and Cys382 are shown. Cys92 is oxidized in the CoA-bound hT1 structure (PDB entry 4c2j). (*b*) Stereo figure of the superposition of CoA-bound human mitochondrial 3-ketoacyl-CoA thiolase (PDB entry 4c2j) chain *C* (blue) with acetoacetyl-CoA-bound *Z. ramigera* thiolase (PDB entry 1m1o) chain *B* (grey). The dotted lines visualize the hydrogen-bond interactions in OAH1 and OAH2. (*c*) PDB entry 4c2j chain *C* (blue) is superposed with acetyl-CoA-bound *Z. ramigera* thiolase chain *B* (PDB entry 1dm3, yellow). In 1dm3 the active-site cysteine Cys89 is acetylated. The two active-site waters of hT1 and bacterial thiolase are coloured red and orange, respectively.

3.5. CoA binding

Apo hT1 crystals were soaked with octanoyl-CoA in order to solve the hT1 structure in complex with a medium-chain fatty acyl-CoA. However, when the structure was solved, CoA molecules were found in the binding site in all subunits of hT1. The electron density of CoA is best defined in chain *C* (Fig. 4). The CoA-binding mode is the same as in the *Z. ramigera* biosynthetic thiolase (PDB entry 1dlv; Modis & Wierenga, 2000) and CT (PDB entry 1wl4; Kursula *et al.*, 2005). The 3′-phosphoadenosine part of the CoA molecule is exposed and is bound in the binding pocket formed by residues His222–Val253 of the loop domain (Fig. 2). When comparing the CoA-bound structure with the apo hT1 structure, the side chain of Arg224 adopts a different conformation. Arg224 makes a cation–π stacking interaction with the adenine moiety of the CoA molecule. The NH2 and NE atoms of Arg224 are at a distance of around 3.2 Å from the N3A (3.2 Å) and C6A (3.2 Å) atoms of the adenine ring, respectively. Furthermore, the NH1 group is hydrogen-bonded (3.1 Å) to the ribose O2B atom of the CoA molecule. The OG1 atom of Thr227 is hydrogen-bonded (3.0 Å) to the N6A atom of the CoA adenine moiety. The pantetheine part of the CoA is surrounded mainly by hydrophobic residues, while the polar atoms interact with water molecules. It makes only one direct hydrogen bond to the protein, which is the conserved interaction between the N8P atom and the peptidyl O atom of Ser251 (Modis & Wierenga, 1999; Fig. 4). There is also a weak conserved hydrogen bond between the Ser251 OG atom and the NP4 atom of CoA.

3.6. Description of the active site

The thiolase active site is buried in the upper part of the thiolase core domain,

underneath the loop domain, close to the tetramerization loop and also close to the dimer interface (Fig. 4). When comparing the hT1 active site with that of the *Z. ramigera* biosynthetic thiolase the geometry of the catalytic site is highly similar and the structural features (active-site loops, catalytic residues and oxyanion holes) involved in the thiolase reaction mechanism are conserved. The catalytic residues Cys92, Asn320, His352 and Cys382 are located in the four active-site loops Nβ3–Nα3, Cβ2–Cα2, Cβ3–Cα3 and Cβ4–Cβ5 with the characteristic sequence fingerprints C*x*S, NEAF, GHP and C*x*G, respectively (Fig. 2). The negatively charged reaction intermediates are stabilized by the hydrogen-bonding networks referred to as oxyanion holes (OAHs; Meriläinen *et al.*, 2009). In thiolases there are two conserved OAHs. OAH1 and OAH2 stabilize the negative charges formed on the thioester carbonyl O atom and the 3-keto carbonyl O atom during the reaction cycle, respectively (Fig. 1). OAH1 in hT1 is formed by His352 and a water molecule (W2129 in the apo structure and W2194 in the CoA-bound structure). There are two conserved active-site water molecules (Fig. 4), which in hT1 are W2127 and W2129 in the apo structure and W2192 and W2194 in the CoA-bound structure. In the apo hT1 structure active site, there is one additional water molecule (W2058 in chain *A*) that mimics the mode of binding of the oxyanion in OAH1, being hydrogen-bonded to His352 NE2 and W2129 as well as to Cys92 SG. OAH2 in hT1 is formed by the main-chain NH groups of the nucleophilic Cys92 and of Gly384 in the C*x*G-loop (Cβ4–Cβ5).

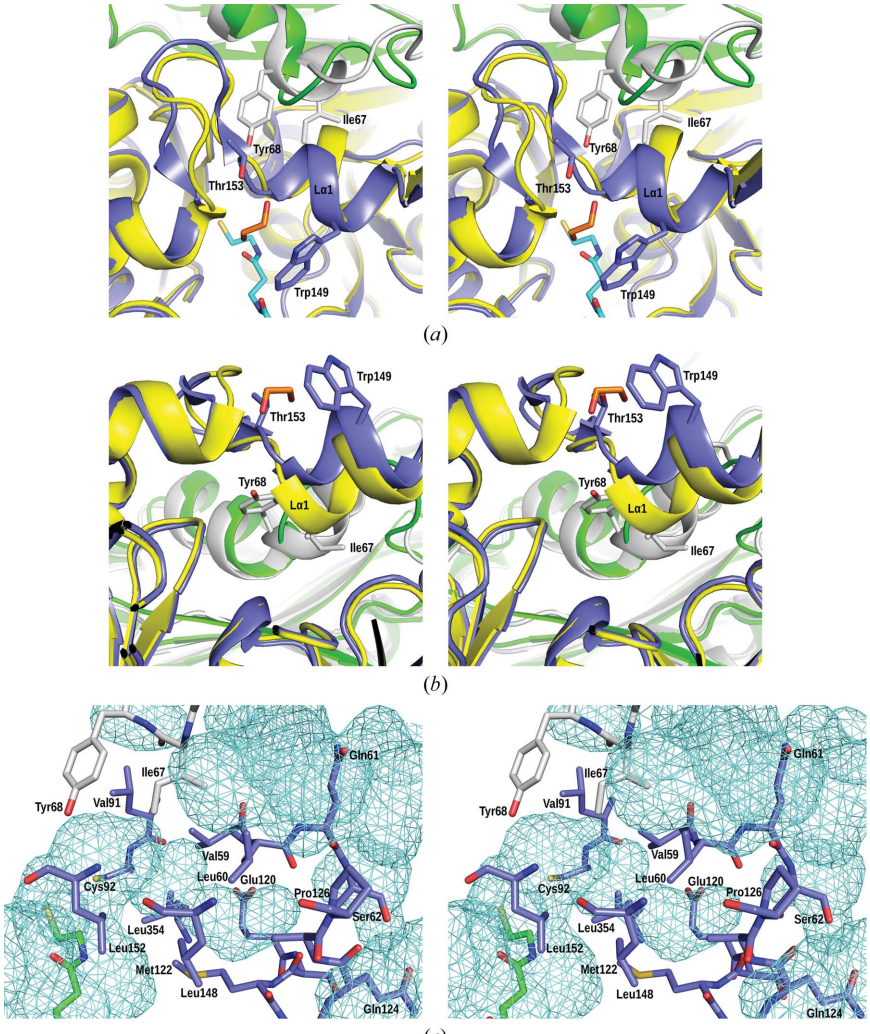

Figure 5
(*a*) Stereo figure of the superposition of short-chain-specific biosynthetic *Z. ramigera* thiolase (PDB entry 1dm3) and medium-chain-specific degradative human mitochondrial 3-ketoacyl-CoA thiolase (PDB entry 4c2j), highlighting the structural differences in the Lα1 helix and the Nβ2–Nα2 loop viewed from the top. Chain *A* and chain *B* of 1dm3 are coloured green and yellow, respectively. Chain *C* and chain *D* of 4c2j are coloured blue and grey, respectively. The ethylene glycol molecule located between Trp149 and Thr153 is shown in orange and the CoA molecule is shown in cyan. (*b*) Side view obtained from (*a*) by rotating 90° about the horizontal axis. (*c*) Putative fatty-acyl tail binding site of the human mitochondrial 3-ketoacyl-CoA thiolase apo structure (PDB entry 4c2k). Chain *A* is shown in blue and chain *B* is shown in grey. Ile67 and Tyr68 of chain *B* form part of the putative fatty-acyl tail binding tunnel. The binding site is surrounded by hydrophobic residues and the end of the binding tunnel is defined by the side chain of Ser62. The protein Connolly surface of the *AB* dimer was calculated with *PyMOL* using the surface-cavity mode with a probe radius of 1.4 Å and is represented as a wireframe. The CoA molecule of the superposed 4c2j structure is shown in green.

When superposing the *Z. ramigera* biosynthetic thiolase in complex with acetoacetyl-CoA (PDB entry 1m1o) with the hT1 structures, the thioester O atom of acetoacetyl-CoA is bound in OAH1 and the 3-keto O atom is bound in OAH2. hT1 is specific for medium-chain and long-chain fatty acids, whereas the *Z. ramigera* biosynthetic thiolase is a short-chain-specific thiolase. The only structural differences in the active site of hT1 (Fig. 5) are in the first α-helix of the loop domain (Lα1) immediately after the tetramerization loop and in the Nβ2–Nα2 dimer interface loop (Gln61–Leu69) of the adjacent subunit. These regions also differ at the amino-acid sequence level when comparing different mammalian T1 proteins with the short-chain-specific CT and T2-thiolases (Fig. 2). In the covering loop between Trp149 and Thr153 there is extra electron density (in each chain of both models) which has been modelled as an ethylene glycol (Fig. 5). The comparison of the acetoacetyl-CoA-bound *Z. ramigera* thiolase with the hT1 structures suggests that the putative fatty-acyl tail binding site is located underneath Lα1 (Fig. 5). Indeed, a cavity analysis outlines a putative fatty-acyl tail binding site shaped by residues from the Nβ2–Nα2 loop of both subunits, Nβ4–Lβ1, Lα1 and the Cβ3–Cα3 loop (Fig. 5). It is lined with hydrophobic residues: Val59, Leu60, Leu91, Met122, Ala125, Pro126, Leu148, Leu152 and Leu354. Ile67 and Tyr68 of the adjacent subunit also point into this tunnel and therefore also form part of the putative fatty-acyl binding site. Polar residues such as

Glu120 and Ser62 line the end of the tunnel, where a buried water molecule (Wat2037) is also bound. The length of this binding site is determined by the Ser62 side chain of the same subunit located at the end of the tunnel. The distance between the side chains of Cys92 and Ser62 is about 15 Å. The substrate-binding site of the *Z. ramigera* thiolase does not have this binding tunnel, in agreement with the notion that it can only accommodate short-chain substrates in its active site (Masamune *et al.*, 1989).

Comparison of the hT1 structure with the yeast peroxisomal degradative AB-thiolase (PDB entry 1afw), which is also a long-chain-specific thiolase, shows that the N-terminal part of the respective loop domain has a totally different conformation (Fig. 6). The dimeric AB-thiolases lack the tetramerization loop, and the N-terminal region of the loop domain has a different fold compared with the tetrameric thiolases. In the AB-thiolase structure there is a 2-methyl-2,4-pentanediol (MPD) molecule bound to the covering loop. In AB-thiolase this loop lacks secondary structure and has high *B* factors, whereas the corresponding region in hT1, Ser147–Pro160, is well ordered and forms the Lα1, Lβ3, Lβ4 hairpin region. Lα1 of hT1 seems to be well stabilized by a hydrogen-bond network and a conserved salt bridge. The carbonyl O atom of Ser151 in Lα1 is hydrogen-bonded to the OH group of Tyr68 in the Nβ2–Nα2 loop of the adjacent subunit. The Ser151 hydroxyl group is hydrogen-bonded to the Ser147 carbonyl O atom and its hydroxyl group is hydrogen-bonded to the Pro126 carbonyl O atom, stabilizing the helix. There is one conserved salt bridge from Lα1 Asp146 to Arg133 in the tetramerization loop of the other subunit of the thiolase dimer. This salt bridge is also present in the *Z. ramigera* thiolase.

The hT1 structure is remarkably similar to the *Z. ramigera* thiolase. However, the active-site water trail extending from the active-site waters to the backside of the *Z. ramigera* molecule is missing in hT1, as it is blocked by the side chains of Val319, Tyr327 and Tyr182 (Fig. 6). This water trail is only present in the very efficient biosynthetic thiolases such as *Z. ramigera* biosynthetic thiolase and human CT-thiolase and not in human T2-thiolase (Haapalainen *et al.*, 2007). It is postulated to be important for the proficient catalytic properties of the biosynthetic thiolases (Kursula *et al.*, 2005). Also similar to the *Z. ramigera* thiolase is the amino-acid sequence and structure of the Cβ1–Cα1 loop. In T2-thiolase (Fig. 2) the sequence is DFP, but in T1-thiolase, as in the *Z. ramigera* CT-thiolase, it is IMG. In T2-thiolase this loop shapes the binding pocket for the 2-methyl group of the 2-methylacetoacetyl-CoA substrate, which is a unique substrate specificity of T2-thiolase. T1 can only degrade unbranched 3-ketoacyl-CoA substrates (Mao *et al.*, 1995).

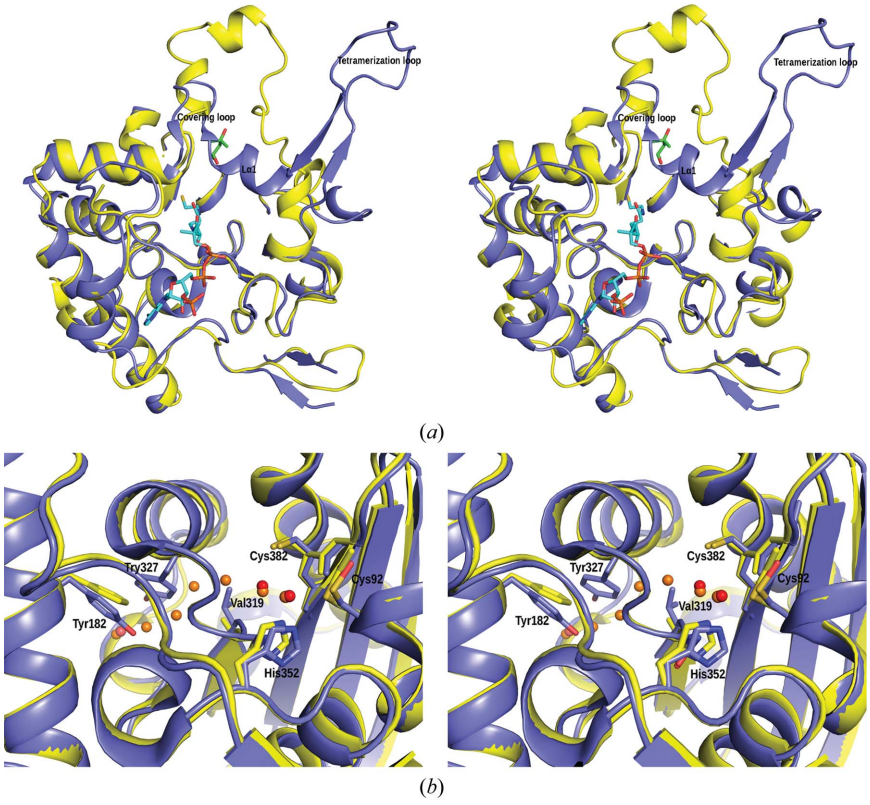

Figure 6
(*a*) Stereo figure of superposition of the tetrameric medium-chain-specific degradative human mitochondrial 3-ketoacyl-CoA thiolase (PDB entry 4c2j) chain *C* (blue) with the dimeric long-chain-specific degradative yeast peroxisomal AB-thiolase (PDB entry 1afw) chain *A* (yellow), highlighting the structural differences in the Lα1 and covering loop region. The 2-methyl-2,4-pentanediol (MPD) in the AB-thiolase structure and CoA in 4c2j are shown as sticks in green and cyan, respectively. The binding site for MPD is predicted to be the binding pocket for the fatty-acyl tail of the yeast peroxisomal degradative thiolase. (*b*) Stereo figure of superposition of the human mitochondrial 3-ketoacyl-CoA thiolase (PDB entry 4c2j) with the *Z. ramigera* biosynthetic thiolase (PDB entry 1dm3), showing that the water trail present in the *Z. ramigera* thiolase cannot be present in the hT1 structure. The *Z. ramigera* thiolase is shown in yellow and the waters in orange; this water trail extends from the active site to the back side of the molecule. hT1 is coloured blue and the waters are shown in red. The 1dm3 water trail is blocked in hT1 by the side chains of Val319 and the two tyrosines Tyr327 and Tyr182. In the *Z. ramigera* biosynthetic thiolase these residues are Ala315, Ala323 and Phe178, respectively.

3.7. Thioesterase activity

Soaking of apo hT1 crystals for 20 min with 1 m*M* octanoyl-CoA resulted in the hT1 complex with CoA owing to the intrinsic thioesterase activity of hT1. Hydrolysis by water of acetylated pig T1 has been reported by Gilbert *et al.* (1981) and also for the *Z. ramigera* thiolase (Thompson *et al.*, 1989; Williams *et al.*, 1992). Detection of the release of free CoA using an HPLC-based assay shows that hT1 is capable of hydrolyzing short-chain, medium-chain and long-chain fatty acyl-CoA molecules (Fig. 7). The thioesterase activity is highest with butyryl-CoA (C4-CoA). The rate of hydrolysis for octanoyl-CoA is about 0.02 s^{-1} at 100 μM substrate concentration and K_m is

about 35 μM. The corresponding k_{cat} for acetoacetyl-CoA cleavage is 15 s^{-1} and that for acetoacetyl-CoA synthesis is 1.4 s^{-1} (Table 2).

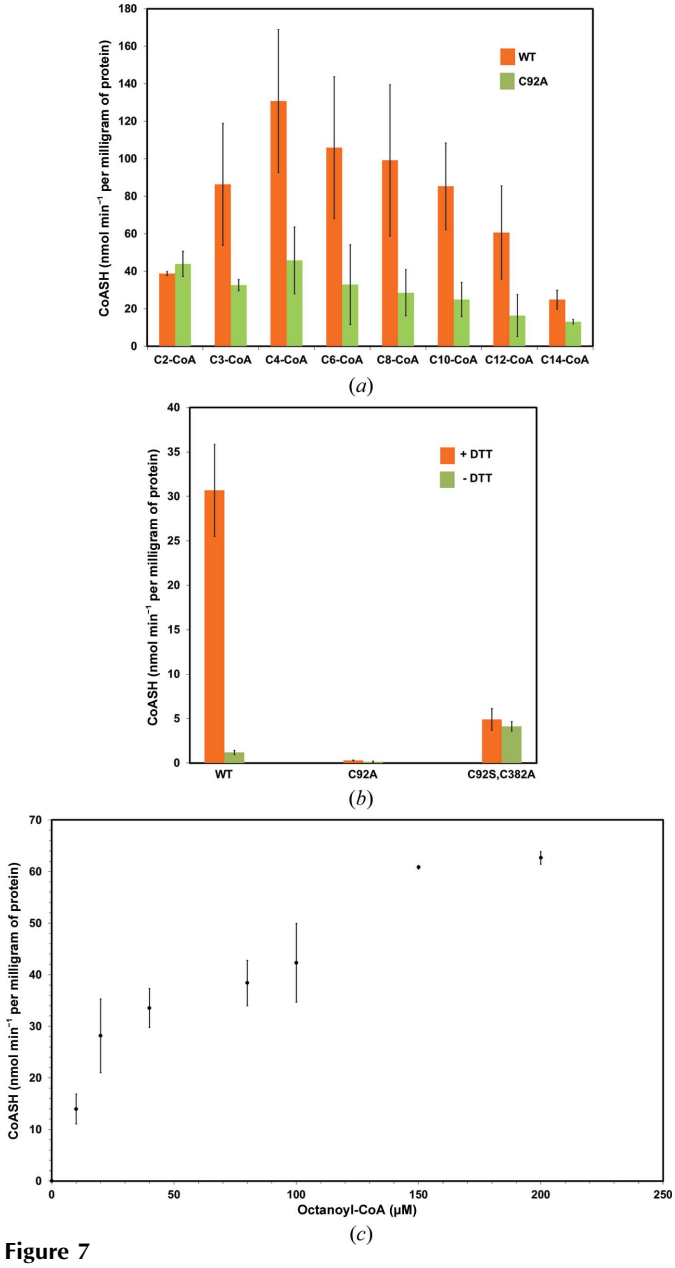

Figure 7
Acyl-CoA thioesterase activity of the wild-type (WT) and C92A and C92S,C382A mutant human mitochondrial 3-ketoacyl-CoA thiolase (hT1) enzymes measured by the production of CoA. (*a*) Acyl-CoA chain-length specificity of the wild-type (WT) and C92A variant hT1 measured with 100 μM of each substrate in the presence of 1 mM DTT. The data are shown as the mean ± s.d. of three experiments. (*b*) Effect of dithiothreitol (DTT) on the acyl-CoA thioesterase activity of WT and C92A and C92S,C382A variant hT1 with octanoyl-CoA. The activity was measured in the presence or absence of 1 mM DTT. The data are represented as the mean ± s.d. of two experiments. (*c*) Michaelis–Menten curve of the thioesterase activity of wild-type hT1 with octanoyl-CoA as substrate measured in the presence of 1 mM DTT. Data are shown as the mean ± s.d. of two to three experiments. The substrates used were C2-CoA, acetyl-CoA; C3-CoA, propionyl-CoA; C4-CoA, butyryl-CoA; C6-CoA, hexanoyl-CoA; C8-CoA, octanoyl-CoA; C10-CoA, decanoyl-CoA; C12-CoA, dodecanoyl-CoA; C14-CoA, tetradecanoyl-CoA.

The presence of reduced DTT is essential in order to be able to measure the thioesterase activity (Fig. 7), consistent with the notion that non-oxidized Cys92 is required. Acetyl-CoA (C2-CoA) is a substrate for the Claisen condensation reaction and incubation with acetyl-CoA leads to the acetylation of the nucleophilic Cys92 and the release of free CoA. The reaction can subsequently proceed in two ways: either (i) by formation of acetoacetyl-CoA or (ii) by hydrolysis of the acetylated Cys92 owing to the instability of the covalent intermediate (Gilbert *et al.*, 1981). However, the hydrolysis reaction of acetylated Cys92 is slow, with a $t_{1/2}$ of 44 min for T1, thereby favouring the formation of acetoacetyl-CoA by transfer of the acetyl group to acetyl-CoA. The half-life of the acetylated T1 enzyme (44 min) is almost 20 times longer than in *Z. ramigera* thiolase (2 min; Thompson *et al.*, 1989).

The enzyme assay carried out with the C92A mutant also reveals the importance of the nucleophilic cysteine for the thioesterase activity. The thioesterase activity of the C92A mutant is at least three times lower compared with the wild-type enzyme. The double mutant C92S,C382A has still some thioesterase activity but is six times less active when compared with wild-type hT1, and this activity is not dependent on DTT. For the *Z. ramigera* thiolase it has been shown that Cys378 is essential for catalysis, especially for the condensation reaction (Williams *et al.*, 1992; Palmer *et al.*, 1991), and the half-life of the acetylated C378G mutant is estimated to be at least 2.5 times longer compared with wild-type *Z. ramigera* thiolase (Palmer *et al.*, 1991). The hT1 analysis indicates that Cys382 is not essential for the hT1 thioesterase activity. The latter observation suggests that the thioesterase mechanism is different from the thiolase reaction mechanism.

3.8. The substrate specificity of T1

The hT1 active-site cavity is larger than the *Z. ramigera* thiolase active-site cavity, as there are relevant structural differences in the 'covering-helix/loop' region as well as in the Nβ2–Nα2 region of the other subunit, near Ile67 and Tyr68 of hT1 (Fig. 5). Superposition of the hT1 structure with the 1m1o structure suggests very nicely where the fatty-acyl chain would point (Fig. 5). The length of the putative fatty-acyl chain binding tunnel is sufficient to be able to accommodate a 14 C atom fatty-acyl chain, which is in good agreement with the acyl-CoA thioesterase experiments (Fig. 7). *In vivo* studies also suggest that the mitochondrial soluble β-oxidation enzymes degrade medium-chain fatty acyl-CoA molecules (with acyl moieties from six to 12 C atoms; Nada *et al.*, 1995). The hypothesis that, for example, the octanoyl tail of the acylated Cys92 binds here refers to the situation in which 3-ketodecanoyl-CoA is the substrate in the degradative direction (Fig. 1), with the thioester O atom binding in OAH1 and the 3-keto O atom binding in OAH2.

3.9. T1 is also important for the synthesis of ketone bodies

Our kinetic data support the hypothesis that hT1 could also be involved in the synthesis of acetoacetyl-CoA for the generation of ketone bodies (Middleton & Bartlett, 1983). The

K_m of the synthetic reaction is relatively high, K_m = 250 μM, but the intramitochondrial concentration of acetyl-CoA can be around 0.5–1 mM (Siess *et al.*, 1976, 1978; Budde *et al.*, 1991). Furthermore, the hT1 Michaelis–Menten parameters (Table 2) are very similar to the T2 Michaelis–Menten parameters for biosynthesis. The importance of hT1 in the synthetic direction also correlates well with the notion that T2 deficiency does not cause a deficiency in ketone bodies (which are synthesized in the liver), but instead T2 deficiency manifests itself as insufficient degradation of 2-methyl organic acids (2-methylacetoacetate, 2-methyl-3-hydroxybutyric acid and tiglylglycine) and ketone bodies (Middleton & Bartlett, 1983; Fukao *et al.*, 2001). The liver is known to contain significant amounts of T1 (Fukao, 2002), which apparently compensates for T2 deficiency in the synthesis of ketone bodies (Middleton & Bartlett, 1983).

3.10. The importance of the oxyanion holes OAH1 and OAH2 for thioesterase activity

One possible explanation for this thioesterase activity is the formation of a covalent intermediate, which is the reverse reaction of the degradative reaction with 3-ketodecanoyl-CoA as the substrate. The C8-acylated enzyme will be activated for hydrolysis by water as the thioester O atom is pointing into OAH2 (Fig. 1). However, the octanoyl-CoA is a product of the thiolytic reaction on 3-ketodecanoyl-CoA (Fig. 1). This product formation requires that the acylated enzyme transfers its acyl group (octanoyl) to CoA and not to water. From the structural studies performed with the *Z. ramigera* biosynthetic thiolase it is evident that after nucleophilic attack by Cys89 on the 3-keto C atom of acetoacetyl-CoA and release of acetyl-CoA the carbonyl group of the acetylated Cys89 can switch from OAH2 to OAH1 by a small rotation of its thioester moiety. For example, it can be noted that in the absence of CoA (PDB entry 1m4s) and in the presence of CoA (PDB entry 1qfl) the thioester O atom of the acetylated enzyme points into OAH1. In the synthetic reaction the thioester O atom of the incoming acetyl-CoA is occupying OAH1 (PDB entry 1dm3) for the acetyl-transfer reaction to take place, and therefore the acetyl carbonyl of the covalently modified Cys89 has to rotate into OAH2 to provide space for the incoming acetyl-CoA. It has been proposed that in the presence of a thioester O atom in OAH1 the catalytic C-terminal cysteine (Cys378) remains activated in its deprotonated form (Meriläinen *et al.*, 2009), which facilitates the Claisen condensation reaction as it is able to abstract a proton from the C2 methyl group of the incoming acetyl-CoA. The Claisen condensation reaction is the reverse reaction of the degradative reaction, using acetyl-CoA instead of CoA as a second substrate, as shown in Fig. 1. The thioesterase formation of CoA from octanoyl-CoA is also the reverse reaction of the 3-ketodecanoyl-CoA degradation, but in this case the acceptor is a water molecule instead of CoA or acetyl-CoA. This reverse reaction may not take place in the same way as the Claisen condensation reaction for the synthesis of acetoacetyl-CoA because Cys382 appears not to be important for thioesterase activity (Fig. 7). For the (slow) thioesterase activity to take place it is in fact sufficient that the thioester O atom of octanoyl-CoA binds in an OAH in such a way that a nearby water molecule can react with the activated thioester C atom (Fig. 1).

In the classical studies on porcine T1 (Gilbert *et al.*, 1981) and on the biosynthetic *Z. ramigera* thiolase (Thompson *et al.*, 1989), it has been shown that the catalytic rates of the degradative and biosynthetic direction are both about tenfold faster for the *Z. ramigera* thiolase compared with T1. Apparently, the transition states of the rate-limiting steps are much better stabilized in the *Z. ramigera* active site than in the T1 active site. These differences in the stabilization of the transition states of the catalytic cycle of the thiolase reaction also mean that the rate-limiting steps in these two enzyme systems are not the same. It has been established that in T1 (Gilbert, 1981) the rate-limiting step in both the degradative reaction and in the synthetic direction is the formation of the acetylated enzyme, whereas for the *Z. ramigera* thiolase (Thompson *et al.*, 1989) it is the enzyme-deacylation step both in the degradative as well as in the synthetic direction.

It was also found that the acetylated enzyme intermediate is more reactive in the *Z. ramigera* thiolase [k(hydrolysis by water) = 50×10^{-4} s^{-1}; Masamune *et al.*, 1989] than in the T1 [k(hydrolysis by water) = 2.6×10^{-4} s^{-1}; Gilbert, 1981]. From these first-order rate constants it is calculated that the half lives of these acetylated enzymes are 44 and 2 min for hT1 and *Z. ramigera* thiolase, respectively. The rate of hydrolysis by water of acetyl-CoA is 5×10^{-7} s^{-1} (Gilbert, 1981), which corresponds to a half life of approximately 100 h under comparable conditions. The faster rates of hydrolysis of the acetylated enzyme indicate that the transition state for hydrolysis by water is better stabilized in the active site of the *Z. ramigera* thiolase compared with T1. Apparently, OAH1 achieves a better stabilization of the reaction intermediate in the *Z. ramigera* acetylated thiolase compared with the T1 active site. An interesting difference with respect to the active-site geometry as deduced from the current structures concerns the presence of a chain of hydrogen-bonded waters that extends from the two catalytic waters involved in OAH1 (Fig. 4) to the back side of the molecule in the *Z. ramigera* thiolase (Kursula *et al.*, 2002) which is absent in hT1 (Fig. 6). It has been speculated that this extensive hydrogen-bonding network is important for the high reactivity of the *Z. ramigera* thiolase (Meriläinen *et al.*, 2009).

4. Concluding remarks

Octanoyl-CoA is the product of the degradative thiolase reaction on the substrate 3-ketodecanoyl-CoA. The rate of thioesterase activity observed with octanoyl-CoA is about 1000-fold slower than the thiolytic cleavage reaction of acetoacetyl-CoA, in which the acetyl group of the acetylated enzyme is transferred to CoA. Two possible explanations have been discussed that rationalize this thioesterase activity. The simplest explanation for the thioesterase activity is to postulate that the CoA part of octanoyl-CoA binds in the CoA-binding pocket as found in the hT1–CoA complex, thereby

allowing the thioester O atom of octanoyl-CoA to bind in either OAH1 or OAH2 (Fig. 1), or both, with different relative occupancies. This mode of binding of the thioester O atom in the OAH will activate the thioester bond for hydrolysis by any water molecule present in the active site (Simón & Goodman, 2010; Kamerlin *et al.*, 2010). Such activation of a carbonyl O atom in an OAH has also been noted in studies of promiscuous activities of a lipase (Carlqvist *et al.*, 2005; Svedendahl *et al.*, 2005; Khersonsky & Tawfik, 2010). An alternative elegant explanation involves the possibility that the nucleophilic cysteine is acylated and that the fatty-acyl tail binds in the hydrophobic tunnel (Fig. 5) extending from the catalytic centre towards Ser62 with its thioester O atom bound in OAH2 (Fig. 1). Indeed, Cys92 in its reduced form is required for thioesterase activity (Fig. 7). However, although various experimental approaches have been tried, it has not been possible to capture the acylated cysteine. In any case, in the normal degradative reaction the acylated T1 enzyme transfers its acyl group preferentially to CoA and not to water. Apparently, the active-site geometry is such that transfer of the acyl group from the acylated enzyme to CoA is more efficient than transfer to water (Fig. 1). Further studies are required to understand why this transfer to CoA is favoured over transfer to water. These structural enzymological studies of hT1 have shown that the medium-chain-length substrate specificity is achieved in a completely different way compared with the peroxisomal homologue. In addition, these studies have provided clear evidence that T1 is important not only as a degradative enzyme but also as a biosynthetic enzyme, being important for the formation of ketone bodies.

Human mitochondrial 3-ketoacyl-CoA thiolase cDNA in pGEM vector was a kind gift from Dr Ohtake, Japan. Erasmus exchange student Maike Eberhart is acknowledged for the initial purification and crystallization of human mitochondrial 3-ketoacyl-CoA thiolase. The research leading to these results received funding from the European Community's Seventh Framework Programme (FP7/2007–2013) under BioStruct-X (grant agreement No. 283570). This research was supported through the Academy of Finland (grant No. 131795 to RKW).

References

Abe, H., Ohtake, A., Yamamoto, S., Satoh, Y., Takayanagi, M., Amaya, Y., Takiguchi, M., Sakuraba, H., Suzuki, Y., Mori, M. & Niima, H. (1993). *Biochim. Biophys. Acta*, **1216**, 304–306.

Anbazhagan, P., Harijan, R. K., Kiema, T. R., Janardan, N., Murthy, M. R., Michels, P. A., Juffer, A. H. & Wierenga, R. K. (2014). *Tuberculosis*, **94**, 405–412.

Antonenkov, V. D., Van Veldhoven, P. P., Waelkens, E. & Mannaerts, G. P. (1997). *J. Biol. Chem.* **272**, 26023–26031.

Antonenkov, V. D., Van Veldhoven, P. P., Waelkens, E. & Mannaerts, G. P. (1999). *Biochim. Biophys. Acta*, **1437**, 136–141.

Artimo, P. *et al.* (2012). *Nucleic Acids Res.* **40**, W597–W603.

Barycki, J. J., O'Brien, L. K., Bratt, J. M., Zhang, R., Sanishvili, R., Strauss, A. W. & Banaszak, L. J. (1999). *Biochemistry*, **38**, 5786–5798.

Bout, A., Franse, M. M., Collins, J., Blonden, L., Tager, J. M. & Benne, R. (1991). *Biochim. Biophys. Acta*, **1090**, 43–51.

Budde, R. J. A., Fang, T. K., Randall, D. D. & Miernyk, J. A. (1991). *Plant Physiol.* **95**, 131–136.

Carlqvist, P., Svedendahl, M., Branneby, C., Hult, K., Brinck, T. & Berglund, P. (2005). *Chembiochem*, **6**, 331–336.

Chen, V. B., Arendall, W. B., Headd, J. J., Keedy, D. A., Immormino, R. M., Kapral, G. J., Murray, L. W., Richardson, J. S. & Richardson, D. C. (2010). *Acta Cryst.* D**66**, 12–21.

Emsley, P. & Cowtan, K. (2004). *Acta Cryst.* D**60**, 2126–2132.

Fukao, T. (2002). *Encyclopedia Of Molecular Medicine*, edited by J. Burchell & J. Taylor-Papadimitriou, pp. 3125–3128. John Wiley & Sons. doi:10.1002/0471203076.emm0319.

Fukao, T., Scriver, C. R., Kondo, N. & T2 Collaborative Working Group (2001). *Mol. Genet. Metab.* **72**, 109–114.

Fukao, T., Song, X. Q., Mitchell, G. A., Yamaguchi, S., Sukegawa, K., Orii, T. & Kondo, N. (1997). *Pediatr. Res.* **42**, 498–502.

Gasteiger, E., Hoogland, C., Gattiker, A., Duvaud, S., Wilkins, M. R., Appel, R. D. & Bairoch, A. (2005). *The Proteomics Protocols Handbook*, edited by J. M. Walker, pp. 571–607. Totowa: Humana Press.

Gehring, U. & Lynen, F. (1972). *The Enzymes*, 3rd ed., edited by P. D. Boyer, pp. 391–405. New York: Academic Press.

Gehring, U., Riepertinger, C. & Lynen, F. (1968). *Eur. J. Biochem.* **6**, 264–280.

Gilbert, H. F. (1981). *Biochemistry*, **20**, 5643–5649.

Gilbert, H. F., Lennox, B. J., Mossman, C. D. & Carle, W. C. (1981). *J. Biol. Chem.* **256**, 7371–7377.

Gouet, P., Courcelle, E., Stuart, D. I. & Métoz, F. (1999). *Bioinformatics*, **15**, 305–308.

Haapalainen, A. M., Meriläinen, G., Pirilä, P. L., Kondo, N., Fukao, T. & Wierenga, R. K. (2007). *Biochemistry*, **46**, 4305–4321.

Haapalainen, A. M., Meriläinen, G. & Wierenga, R. K. (2006). *Trends Biochem. Sci.* **31**, 64–71.

Horecker, B. L. & Kornberg, A. (1948). *J. Biol. Chem.* **175**, 385–390.

Kabsch, W. (2010). *Acta Cryst.* D**66**, 125–132.

Kamerlin, S. C. L., Chu, Z. T. & Warshel, A. (2010). *J. Org. Chem.* **75**, 6391–6401.

Khersonsky, O. & Tawfik, D. S. (2010). *Annu. Rev. Biochem.* **79**, 471–505.

Krissinel, E. & Henrick, K. (2004). *Acta Cryst.* D**60**, 2256–2268.

Kursula, P., Ojala, J., Lambeir, A. M. & Wierenga, R. K. (2002). *Biochemistry*, **41**, 15543–15556.

Kursula, P., Sikkilä, H., Fukao, T., Kondo, N. & Wierenga, R. K. (2005). *J. Mol. Biol.* **347**, 189–201.

Larkin, M. A., Blackshields, G., Brown, N. P., Chenna, R., McGettigan, P. A., McWilliam, H., Valentin, F., Wallace, I. M., Wilm, A., Lopez, R., Thompson, J. D., Gibson, T. J. & Higgins, D. G. (2007). *Bioinformatics*, **23**, 2947–2948.

Laskowski, R. A., MacArthur, M. W., Moss, D. S. & Thornton, J. M. (1993). *J. Appl. Cryst.* **26**, 283–291.

Mao, L. F., Chu, C., Luo, M. J., Simon, A., Abbas, A. S. & Schulz, H. (1995). *Arch. Biochem. Biophys.* **321**, 221–228.

Masamune, S., Walsh, C. T., Sinskey, A. J. & Peoples, O. P. (1989). *Pure Appl. Chem.* **61**, 303–312.

Mathieu, M., Modis, Y., Zeelen, J. P., Engel, C. K., Abagyan, R. A., Ahlberg, A., Rasmussen, B., Lamzin, V. S., Kunau, W. H. & Wierenga, R. K. (1997). *J. Mol. Biol.* **273**, 714–728.

Mathieu, M., Zeelen, J. P., Pauptit, R. A., Erdmann, R., Kunau, W. H. & Wierenga, R. K. (1994). *Structure*, **2**, 797–808.

McCoy, A. J., Grosse-Kunstleve, R. W., Adams, P. D., Winn, M. D., Storoni, L. C. & Read, R. J. (2007). *J. Appl. Cryst.* **40**, 658–674.

Meriläinen, G., Poikela, V., Kursula, P. & Wierenga, R. K. (2009). *Biochemistry*, **48**, 11011–11025.

Middleton, B. (1973). *Biochem. J.* **132**, 731–737.

Middleton, B. (1974). *Biochem. J.* **139**, 109–121.

Middleton, B. & Bartlett, K. (1983). *Clin. Chim. Acta*, **128**, 291–305.

Miyazawa, S., Furuta, S., Osumi, T., Hashimoto, T. & Ui, N. (1981). *J. Biochem.* **90**, 511–519.

Modis, Y. & Wierenga, R. K. (1999). *Structure*, **7**, 1279–1290.
Modis, Y. & Wierenga, R. K. (2000). *J. Mol. Biol.* **297**, 1171–1182.
Murshudov, G. N., Skubák, P., Lebedev, A. A., Pannu, N. S., Steiner, R. A., Nicholls, R. A., Winn, M. D., Long, F. & Vagin, A. A. (2011). *Acta Cryst.* D**67**, 355–367.
Nada, M. A., Rhead, W. J., Sprecher, H., Schulz, H. & Roe, C. R. (1995). *J. Biol. Chem.* **270**, 530–535.
Palmer, M. A., Differding, E., Gamboni, R., Williams, S. F., Peoples, O. P., Walsh, C. T., Sinskey, A. J. & Masamune, S. (1991). *J. Biol. Chem.* **266**, 8369–8375.
Riddles, P. W., Blakeley, R. L. & Zerner, B. (1983). *Methods Enzymol.* **91**, 49–60.
Schulz, H. & Staack, H. (1981). *Methods Enzymol.* **71**, 398–403.
Seubert, W., Lamberts, I., Kramer, R. & Ohly, B. (1968). *Biochim. Biophys. Acta*, **164**, 498–517.
Siess, E. A., Brocks, D. G. & Wieland, O. H. (1976). *FEBS Lett.* **69**, 265–271.
Siess, E. A., Brocks, D. G. & Wieland, O. H. (1978). *Hoppe Seylers Z. Physiol. Chem.* **359**, 785–798.
Sikkilä, H. (2004). Masters thesis. Department of Biochemistry, University of Oulu, Finland.
Simón, L. & Goodman, J. M. (2010). *J. Org. Chem.* **75**, 1831–1840.
Staack, H., Binstock, J. F. & Schulz, H. (1978). *J. Biol. Chem.* **253**, 1827–1831.
Svedendahl, M., Hult, K. & Berglund, P. (2005). *J. Am. Chem. Soc.* **127**, 17988–17989.
Thompson, S., Mayerl, F., Peoples, O. P., Masamune, S., Sinskey, A. J. & Walsh, C. T. (1989). *Biochemistry*, **28**, 5735–5742.
Uchida, Y., Izai, K., Orii, T. & Hashimoto, T. (1992). *J. Biol. Chem.* **267**, 1034–1041.
Williams, S. F., Palmer, M. A., Peoples, O. P., Walsh, C. T., Sinskey, A. J. & Masamune, S. (1992). *J. Biol. Chem.* **267**, 16041–16043.
Zeelen, J. P., Hiltunen, J. K., Ceska, T. A. & Wierenga, R. K. (1994). *Acta Cryst.* D**50**, 443–447.